The formation and implications of giant blocks and fluid escape structures in submarine lateral spreads

Nan Wu[1]*, Christopher A-L. Jackson[1], Howard D. Johnson[1], David M. Hodgson[2], Michael A. Clare[3], Harya D. Nugraha[1], Wei Li[4]

[1]Basins Research Group (BRG), Department of Earth Science & Engineering, Imperial College, Prince Consort Road, London, SW7 2BP, UK

[2]School of Earth and Environment, University of Leeds, Leeds, LS2 9JT, UK

[3]National Oceanography Centre, Southampton SO14 3ZH, UK

[4]South China Sea Institute of Oceanology, Chinese Academy of Sciences, China

*Email: n.wu16@imperial.ac.uk

Abstract

Lateral spread (or 'spreading') and submarine creep are processes that occur near the headwalls of both terrestrial landslides and submarine mass-transport complexes (MTCs). Both submarine creep and spread deposits may contain giant (km-scale) coherent blocks, but their transport processes remain poorly constrained. Here we use 2D and 3D seismic reflection data to determine the geometry, scale, and origin of an ancient (Late Miocene) mass-transport complex (MTC) located in the Kangaroo Syncline, offshore NW Australia. We show that this large remobilised mass of carbonate ooze is c. 170-300 m thick and covers an area of at least c. 1050 km^2. The deposit is defined internally by two distinct seismic facies: (i) large, upward-tapering blocks (up to 210-300 m thick, 170-210 m wide, and 800-1200 m long) with negligible internal deformation, which decrease in height and spacing along the transport direction (identical, but *in situ*, seismic facies forms undeformed slope material immediately updip of the deposit headwall); and (ii) troughs (160-260 m thick, 190-230 m wide and 800-1200 m long) comprising moderately deformed strata, which contain 'v'-shaped, pipe-like structures that extend upwards from the inferred basal shear surface to the top surface of the MTC. The lack of deformation within the blocks, and their correlation to adjacent in-situ deposits, suggests they underwent very limited transport (c. 50 m-70 m). The relatively high degree of deformation within the intervening troughs is attributed to the vertical expulsion of fluids and sediment during hydraulic failure of the sediment mass. We

present a hydraulic failure model that accounts for the styles and patterns of intra-MTC deformation process. This model invokes evacuation of the lower slope by a pre-cursor MTC that formed the space to trigger the lateral spread event. Our study provides new insights into the genesis and rheology of subaqueous lateral spreads, enabling improved assessments of the threats posed to critical seafloor infrastructure. The genetic links identified between mass wasting and spatially-focused fluid flow indicate that, as well as disturbing the deep seafloor, submarine landslides may also create important deep-sea biodiversity hotspots.

Keywords: spread, slope failure, geohazard, mass-transport complex (MTC), submarine landslide, Exmouth Plateau, NW Shelf, Australia

Introduction

Mass-transport complex (MTC) is a broad term typically used to describe slope failure deposits resulting from creep, spread, slide, slump, and debris flow processes (Figure 1; Varnes, 1978; Nemec, 1990). MTCs are responsible for transporting large volumes of sediments from basin margins to the adjacent basin floor, often during single catastrophic events (e.g. Posamentier and Martinsen, 2011). Because of their size, the generation and emplacement of MTCs play a key role in shaping and controlling the stratigraphic evolution of continental margins around the world (Posamentier and Martinsen, 2011). MTCs can initiate and translate over very low-angle seafloors by hydroplaning, with sediments in the overlying failure mass partly or fully disaggregated to form a genetically related debris flow (De Blasio and Elverhoi, 2011). Partial disaggregation can result in the formation and emplacement of relatively coherent, largely undeformed blocks (Micallef et al., 2007; Jackson, 2011; Alves, 2015; Li et al., 2016) that may trigger tsunamis (Tappin, 2010), could damage or destroy seabed infrastructure (Masson et al., 2006; Urlaub et al., 2013), be a pre-cursor for subsequent slope failure events (i.e. Lee and Chough, 2001; Li et al., 2016), or increase the slope stability by reducing gravitational potential (Shillington et al., 2012). The nature of any impacts to seafloor structures, and also the potential for tsunamigenesis, strongly depend on the degree of landslide disaggregation, the volume and strength of the failed mass, its mobility, speed and direction of movement (e.g. Watts et al., 2005; Zakeri, 2009; Zhu and Randolph, 2010; Randolph and White, 2012; Dutta and Hawlader, 2019). For instance, highly mobile, yet relatively thin debris flows have toppled oil and gas platforms, and ruptured pipelines in the Gulf of Mexico (e.g. Chaytor et al., 2020). Conversely, much larger, deep-

seated (i.e. relatively thick), and yet limited run-out MTCs triggered by the 2011 Tōhoku-Oki earthquake (M_w 9.1) caused no discernable damage to seafloor telecommunication cables (e.g. Strasser et al., 2013; Pope et al., 2017). Therefore, differentiating the nature of slope failure processes is a key element in assessing their risk to coastal communities and critical seafloor infrastructure.

Submarine creep (or 'spreading') and lateral spreading are gravity-driven processes that occur near the headwall area of sediment failure in marine (syn.: 'submarine spread') and terrestrial (landslides) settings, respectively (Figure 1). Submarine creep is defined as a slow, gravity-driven, downslope motion or post- or syn-depositional deformation of a sediment mass (Silva and Booth, 1984; Nemec, 1990). The deposits of submarine creep may contain giant coherent blocks that are up to c. 300 m high and c. 4 km wide (e.g. Li et al., 2016).

Subaqueous spread (also known as gravitational spreading and lateral spreading; Varnes, 1978; Savage and Varnes, 1987) is another type of gravity-induced failure. First defined in terrestrial settings as 'lateral spreading', this type of failure is triggered by subsurface liquefaction and the formation of an intra-stratal weak zone, above which the failed mass translates (Varnes, 1978). Commonly, these masses are stretched and broken up into internally coherent blocks (Figure 1). A key characteristics of spreads is that they can occur above a very gently-dipping (*ca.* < 1°) failure surface (Cruden and Varnes, 1996; Micallef et al., 2007). A subaqueous spread can have a lateral displacement of only a few tens of metres (Micallef et al., 2007). Despite this, onshore analogues indicate that the emplacement of spread-related blocks could be extremely hazardous. For example, a spread and its associated debris occurred in Palu, Indonesia, following an earthquake in September 2018, leaving >2000 people dead and c. 1300 people missing (Bradley et al., 2019; Watkinson and Hall, 2019). Subaqueous spread-related deposits have received less attention than their terrestrial counterparts, despite 3D seismic reflection data being an excellent tool to resolve the external and internal geometry, and origin of this particular type of submarine landslide (Micallef et al., 2007). Although the deposits of submarine creep and spread have similar external geometries and internal seismic facies, they are different failure process and are typically not considered part of a continuum; i.e. creep would not transform into spread, or vice versa.

Many landslide hazard assessments are based solely on plan-view imaging using multibeam bathymetric surveys (e.g. Geertsema et al., 2018). While incredibly valuable, such surveys the

lack subsurface information required to identify and diagnose the style and depth of landslide failure, and the nature of internal deformation. Here we demonstrate the value of high resolution 2D and 3D seismic reflection data to complement and advance modern seafloor studies of MTCs. Our aim is to evaluate the morphology, internal structure, kinematics, origin and geohazard risk of a large submarine MTC using a high-quality, 3D and 2D seismic reflection dataset from the NW Shelf, offshore Australia. Using these data, we can quantify the height and spacing of the contained blocks, whereas a detailed kinematic analysis of intra-MTC structures allows the transport direction to be determined. The study also aims to offer a better understanding of spread initiation, translation, and deposition, which will help to build a more comprehensive model for submarine mass failures and to help understand, and hence inform mitigation of the associated geohazard risk.

Geological setting

The Exmouth Plateau is located offshore NW Australia, c. 900 km south of the tectonically-active boundary between the Australian and Eurasian tectonic plates (Fig. 2a, 2b) (Hengesh et al., 2012; Hengesh et al., 2013). The Exmouth Plateau is c. 600 km long and c. 350 km wide, and is presently located in water depths of 1100-5000 m (Falvey and Veevers, 1974; Exon et al., 1992; Hengesh et al., 2013) (Figure 2a). This study focuses on the Upper Miocene to Holocene passive margin mega-sequence (Figure 2c). This interval records the relatively slow deposition (c. 0.02 mm/yr) of very fine-grained carbonate in bathyal (200-2000 m) water depths (Exon et al., 1992; Haq et al., 1992; Maher and Thompson, 1999). Cores from Ocean Drilling Program (ODP) wells 762 and 763 have established that the dominant lithology in this interval is nannofossil-rich carbonate ooze (Exon et al., 1992; Haq et al., 1992; Boyd et al., 1993). These deposits are characterised by high porosities (c. 70%) and high water saturations (c. 40%), and by an overall low strength profile (<20kPa) (von Rad, 1992; see Figure 5 from Hengesh et al., 2012). These physical properties increase the slope instability and related geohazard risk of the Exmouth Plateau area. Prolonged slope instability is recorded in the presence of large (e.g. c. 500km^3 gorgon slide; Hengesh et al., 2012), stacked, slope-to-basin floor MTCs in the upper part (i.e. post-Oligocene) of the passive margin mega-sequence (Hengesh et al., 2012; Scarselli et al., 2013; Nugraha et al., 2018; Nugraha et al., 2019). The study area is located in the axis of the Kangaroo Syncline, between the Exmouth Plateau to the west and the NW Shelf to the east (Figure 2a, 2d). The stratigraphic interval under

investigation extends upwards from Horizon H1 (base) to the seabed (top) (Figure 2c, 3a-c). Horizon H1 (Figure 3b) is a regionally mappable unconformity that defines the base of the Late Miocene, and which records collision of the Australian and Eurasian plates (Boyd et al., 1993; Hull and Griffiths, 2002). The Late Miocene to Holocene succession thickens basinwards into the axis of the Kangaroo Syncline, and thins to the east and west, towards the NW Shelf and the crest of Exmouth Plateau, respectively (Nugraha et al., 2018).

Dataset and Methodology

In this study we use two types of seismic reflection data provided by Geoscience Australia (http://www.ga.gov.au/nopims): (i) up to c. 500 km long, 2D seismic reflection surveys, which were collected between 1993 and 2005; and (ii) a 3D seismic reflection survey (Willem 3D seismic survey), which was acquired by Veritas DGC Australia in 2006. The Willem 3D seismic survey covers a total area of c. 2628 km^2, extending along the Exmouth continental slope and across the lower slope into the Kangaroo Syncline (Figure 2a-b). A downward decrease and increase in acoustic impedance are expressed as blue (negative) and red (positive) reflection events, respectively (Figure 3a). We estimate the spatial resolution of the Willem seismic survey using the frequency content (c. 60 Hz decreasing to c. 40 Hz) and average seismic velocity (1500 m/s decreasing to 2000 m/s) between the seabed and H1. Based on these data, we calculate an approximate spatial resolution of 6.25 m at the seabed, decreasing to 11 m near the base of the studied interval. This imaging quality is sufficient to map, at relatively high-resolution, the geometry of structural features (e.g. scours, faults, etc) immediately below and within the studied MTC.

We adopt the seismic-stratigraphic framework of Nugraha et al. (2018), which is based on their analysis of the Exmouth Plateau, c. 50 km SW of the study area (Figure 2a). Our study interval falls within SU3 of Nugraha et al. (2018), within which we map four horizons based on the seismic continuity, amplitude, and frequency/spacing, as well as the seismic facies characteristics of the packages they bound. The lithology and geotechnical properties (i.e. water content, porosity, shear strength, etc.) of the studied stratigraphic interval are inferred from ODP Wells 762 and 763, which are located c. 300 km SW of the study area where they penetrate a similar seismic-stratigraphic succession. We extracted seismic attributes, such as variance and amplitude contrast (see Supporting Information Appendix 1 for explanation), from the 3D seismic reflection dataset to determine the external geometries and

geomorphology of the imaged deep-marine deposits (Chopra and Marfurt, 2007; Brown, 2011). The dimensions of the MTC-hosted blocks have been quantitatively analysed based on their morphological characteristics: (i) *block height*, which is the height between the crest and base of the blocks (i.e. the MTC basal shear surface); (ii) *block spacing*, which is the spacing between the middle of the crests of two adjacent blocks; (iii) *block tip angle*, which is the angle between the block tip and vertical; and (iv) *block friction angle*, which is the angle between the side of the blocks relative to their base surface (see Figure 6b).

Seismic-stratigraphic analysis

We identified and mapped four key horizons (H1-H4) in this study based on their strong amplitude, continuity (i.e. they are regionally mappable and extend across the study area), and stratigraphic distribution (i.e. they are relatively evenly distributed throughout the stratigraphic succession of interest). Horizon H1 (Figure 2b) is a regionally mappable unconformity that defines the base of the Late Miocene, and which formed as the result of the collision of the Australian and Eurasian plates (Boyd et al., 1993; Hull and Griffiths, 2002).

SU-1 and SU-2

We divide the studied stratigraphic interval into three seismic units (SU-1-3). SU-1 is c. 500 m thick near the axis of the Kangaroo syncline, thinning westward and eastward to c. 200 m. SU-1 contains packages of chaotic, medium- to high-amplitude seismic reflections interpreted as stacked MTCs (Figure 3b-c) (Hengesh et al., 2012; Nugraha et al., 2018). SU-2 is thinner than SU-1, but also varies in thickness, being slightly thicker near the centre of the Kangaroo Syncline (c. 60 m) and thinning gradually westward and eastward to c. 30 m (Figure 3b). SU-2 contains two distinct seismic facies: (i) continuous, low- to medium-amplitude, sub-parallel seismic reflections in the east; and (ii) discontinuous to chaotic seismic facies in the centre and west (Figure 3b-c). The continuous seismic facies is interpreted as slope-to-basinfloor, carbonate ooze deposits, whereas the more discontinuous seismic facies is interpreted as deformed carbonate ooze drape deposits (Nugraha et al., 2018). Variance attribute-based analysis of the base of SU-2 (Horizon H2) in the central part of the study area reveals a concentrated high variance response with circular shape in an NW-SE linear trend (Figure 5a). These high variance circles form bulges in seismic section that are c. 30-70 m in diameter, disaggregating the overlying strata (see the seismic section in Figure 5a). Based on their size,

geometry, and distribution, these circular bulges are interpreted as fluid expulsion-related pockmarks (e.g. Plaza-Faverola et al., 2011). Fluid escape features such as these are common on the Exmouth Plateau (i.e. Velayatham et al., 2018; Velayatham et al., 2019).

SU-3

SU-3 is c. 500 m thick in the axis of the Kangaroo Syncline, gradually thinning westward due to truncation below MTC 3 (Figure 4a, 4b). We identify three distinct seismic facies in SU-3, which we describe below (pre-MTC 3, MTC 3, and MTC 2; Figure 3b).

Pre-MTC 3

The pre-existing interval defines the eastern part of SU-3 and is characterised by a thin (70 ms TWT; 25% of the total thickness of SU-3) package of chaotic to discontinuous, low- to medium-amplitude seismic reflections at its base, which is overlain by a thick (170 ms TWT; 75% of the total thickness of SU-3) package of continuous-to-locally slightly wavy, low- to medium-amplitude seismic reflections (Figure 3c). The chaotic seismic facies is interpreted as an MTC (MTC 1), whereas the continuous seismic facies likely represents carbonate ooze (Figure 3b, 3c) (Nugraha et al., 2018).

MTC 3

Description

MTC 3 defines the central part of SU-3, near the axis of the Kangaroo Syncline, where the seafloor presently dips very gently (c. 0.4°) (Figure 4b). Approximately 1050 km^2 of MTC 3 is imaged in the 3D seismic data, although 2D seismic data show the deposit covers c. 3600 km^2 (Figure 4a, 4b; Figure 5b, 5c, 5d). We describe MTC 3 with respect to the following features: (i) the geometry of its basal shear surface and seismic facies of its substrate, (ii) the seismic facies and geometrical characteristics of its contained blocks and troughs, and (iii) its overall geometry and the geometry of its top surface.

(i) The basal shear surface and substrate

The basal surface of MTC 3 is characterised by a continuous, high-amplitude, positive seismic reflection (Figure 6a). In the east, this surface merges with the basal shear surface of MTC 1 (Figure 6a). The basal surface of MTC 3 does not contain any seismic-scale erosional features such as scours, striations, or grooves (Figure 5c, 5d) (e.g. Bull et al., 2009a; Sobiesiak et al., 2018). As such, it is not easy to determine the MTC transport direction. However, the surface

defines a sharp boundary between different facies (i.e. weakly deformed below and very chaotic above), and the high-amplitude character supports an interpretation of a basal shear surface (e.g. Wu et al., 2019). The 60 ms TWT thick (c. 60 m) unit immediately underlying and representing the substrate of MTC 3 ranges from discontinuous and moderately deformed near the eastern-margin of MTC 3, to chaotic and highly deformed near the proximal part of the deposit (Figure 6a, 6b).

(ii) Blocks and troughs

Map-view images show that MTC 3 contains parallel to sub-parallel, block-shaped packages (Figure 5c, 5d). In seismic cross sections, these form ridge-shaped blocks flanked by troughs (Figure 6b). The blocks are 210-300 m high, 170-210 m wide, and 800-1200 m long are relatively undeformed (Figure 6b). The intervening troughs are 160-260 m high, 190-230 m wide, 800-1200 m long, and are defined by a very chaotic, variable-amplitude seismic facies.

All the blocks contain two distinct seismic facies that are similar to those defining undeformed slope strata outside of the MTC (Figure 6a, 6b). Seismic reflection within the blocks are sub-horizontal and are approximately parallel to the basal shear surface and underlying substrate strata. Three seismic reflections, intra-block reflections a-c, are identified within the blocks, which can be correlated with confidence from block-to-block over a large area (seismic reflection a-c; Figure 6b). However, the blocks become more disaggregated, and their external form become less pronounced, adjacent to the headwall in the E and adjacent to its toe in the SW. Downslope, intra-block reflections a-c become harder to identify and trace (Figure 6c). The blocks ultimately become extremely chaotic in the distal part of MTC 3, showing similar facies to MTC 1 (Figure 6c). Upslope, the relationship between the blocks and the undeformed strata show a clear increasing deformation systematically eastward (Figure 6a).

The average tip angle of the blocks is c. 38°, with little variability about this value (Figure 6d). The angle of the tip to the basal shear surface ranges from 55-80° (average 71°) (Figure 6d). The height of the blocks gradually decreases downslope to the SW towards the distal end of MTC 3, from c. 290 m to c. 190 m (Figure 6e). Block spacing increases towards the SW, from c. 610 m near the centre to c. 760 m near the distal region of MTC 3 (Figure 6e).

The intra-block troughs are characterised by moderately discontinuous to chaotic seismic facies (Figure 6b). By blending variance and amplitude data we see that the troughs contain

numerous ‘v’-shaped, vertical to sub-vertical, pipe-liked structures that extend from the basal shear surface of MTC 3 to its top. We refer to these c. 280 m tall, up to 100 m diameter features as ‘subvertical deformation zones’ (SDZs) (Figure 7a). Within troughs, seismic reflections are mostly sub-horizontal and discontinuous, the edge of the reflections can be as steep as 50° near the trough margin (Figure 7a). Locally, where the magnitude of intra-trough deformation is low, we can trace seismic reflections from within the troughs into adjacent blocks (see the coloured dots in Figure 7a). The width of the VDZs increase upward, from c. 40 m at their narrowest basal point to up a few hundreds of metres at their tops (Figure 7b and c).

(iii) Top surface

The top of MTC 3 is characterised as a rugose low-amplitude, positive seismic reflection. The crests of intra-MTC blocks define locally positive relief that are onlapped by overlying reflections, whereas intervening troughs define concave-up structural lows (Figure 6a, 6b). The VDZs extends throughout the vertical extent of the trough, and reflections onlap the blocks (Figure 7a).

Interpretation

The similarity in the seismic facies succession characterising the intra-MTC blocks and the undeformed strata (i.e. a thin MTC overlain by largely undeformed, slope-to-basinfloor strata) suggest the former are derived from the latter. This is supported by the blocks in the eastern part of MTC 3 being the same thickness as the laterally adjacent, largely undeformed interval. We therefore interpret the boundary between MTC 3 and the undeformed strata is the MTC headwall. The fact we can correlate the intra-MTC seismic horizons (reflection a-c; Figure 6a, b) within the blocks and flanking, more highly deformed troughs, suggest that the blocks were initially transported as a coherent mass. The continuity of the intra-block reflections also indicate that the blocks were only weakly deformed during the transport.

We interpret that the westward decrease in block height and spacing, normal to the broadly NE-trending headwall, suggest MTC 3 was translated westwards, approximately perpendicular to the depth contour of the interpreted base of the MTC 3 (Figure 5b, 5d). We also note that the amount of deformation below MTC 3, inferred from the thickness of the highly deformed package, increases westwards at the transition from beneath the relatively

thin MTC 1, which forms part of the pre-existing, broadly undeformed slope strata, to below the relatively thick MTC 3. The low degree of internal deformation, limited distance from the headwall, and lack of kinematic indicators, supports an interpretation that the blocks moved a limited horizontal distance. Therefore, we suspect that the relatively highly deformed nature of the substrate near the proximal part of MTC 3 may not have been directly caused by shearing of the substrate by the overlying mass. We instead interpret that this deformation occurred due to the presence and catastrophic failure of an overpressured substrate by liquefaction or strain softening, which both would have caused intense stratal disruption. Similar liquefaction-driven seismic facies (i.e. medium- to high-amplitude, chaotic seismic reflections) are described in the literature (e.g. Ogata et al., 2014).

The moderately-deformed reflections defining the VDZs indicate modest internal deformation within these areas. We infer that the VDZs represent vertical fluid migration conduits, which drove fluid expulsion from the underlying, over-pressured substrate (e.g. Moss and Cartwright, 2010; Løseth et al., 2011; Cartwright and Santamarina, 2015). The overlying elliptical depressions, which define structural lows along the top of MTC 3, reflect overburden collapse due to the expulsion, upward migration, and expulsion of deeper material. Seismic reflections onlapping blocks protruding from the top surface of MTC 3 may represent the extruded sediments or subsequently deposited deep-water sediment (e.g. Clari et al., 2004; Roberts et al., 2010; Watkinson and Hall, 2019).

MTC 2

MTC 2 occurs in the western part of SU-3 (Figure 4b, 5c-d). This deposit is deeply eroded on its NW margin by a subsequent mass failure event (MTC 4), and is hard to differentiate from MTC 3 in the NE (Figure 4b, 5d). However, the boundary between MTC 2 and 3 can be inferred from their slightly differing seismic facies; MTC 3 is defined by an overally higher-amplitude, blockier seismic facies, whereas MTC 2 is defined by overall lower-amplitude, chaotic seismic facies (Figure 3a-c). MTC 2 has an NW-trending headwall (Figure 8a) and NE-SW trending lateral margins (Figure 8b), and comprises low- to very low-amplitude, chaotic reflections. In the northern part of the Kangaroo syncline, MTC 2 increases in thickness away from its headwall, from c. 70 ms near its headwall (Figure 8a) to c. 200 ms further NE (Figure 8c). The orientation of the headwall scarp and lateral margins suggest that MTC 3 was transported towards the NNE, following the overall dip of the Kangaroo Syncline (Figure 4b).

Stratigraphic evolution

Based on the observations made above, we propose that the study area has experienced several episodes of slope failure-driven erosion and deposition (Figure 9). First, multiple, stacked MTCs were deposited (SU1; Figure 9a) that were subsequently draped by carbonate ooze (SU-2; Fig. 9b). Gas or fluids, sourced from deeper stratigraphic levels, migrated upward into SU-2 (Figure 9b). During the initial stage of SU-3 deposition, an MTC was emplaced (MTC 1), which was overlain by a thick, carbonate ooze-bearing sequence (Figure 9c). MTC 2 was subsequently emplaced in the west of the study area (Figure 9d). The removal of sediment during the evacuation of MTC 2 likely had a debuttressing effect, promoting subsequent slope failure and the triggering of MTC 3 through removal of lateral and down-slope confining support (Figure 9d). As a result of overpressure released by slope failure, sediments extruded from below MTC 3 were transported upward through, and deposited on top of, the overlying mass. MTC 4 was subsequently emplaced in the west of the study area on top of MTC 3, followed by draping of the entire succession by carbonate ooze (Figure 9e).

Discussion

Was MTC 3 emplaced by a creep or spread?

Creep is a gravity-driven process, with the updip margins defined by retrogressively formed faults and folds (Lee and Chough, 2001; Li et al., 2016). In contrast, spreading occurs above a pre-cursor failure surface, with the failed mass translating laterally and being broken into blocks and troughs that are bounded by internally generated faults (Micallef et al., 2007). Subaqueous creep has been reported from relatively steep slopes (>3°) (i.e. Silva and Booth, 1984; Shillington et al., 2012), whereas subaqueous spread is reported from gentler slopes occur (<1°) (i.e. Micallef et al., 2007). Although we have not undertaken a balanced structural restoration to investigate the slope dip at the time of MTC 3 emplacement, it is likely that, given its current position beneath the present basin floor, some c. 300 km from the Late Miocene shelf margin, it was deposited on a gently dipping slope (<1°). The coherent blocks within MTC 3 occur above a low-angle failure surface, suggesting gravity played only a minor role in their formation, as well as that of the MTC in which they are contained. The blocks are also bound by numerous sub-parallel faults that are of very similar dip; such features are strongly characteristic of the deposits of spreads, rather than creep (Micallef et al., 2007).

MTC 3 emplacement model

Stage 1: Priming

Before the emplacement of MTC 3, the basal shear surface of MTC 1 may have represented a hydraulic boundary between the overlying c. 300 m thick sediment pile, and the underlying substrate, defined by sharp decrease in permeability and density (i.e. Madhusudhan et al., 2017; Wu et al., 2019) (Figure 10a, 10b). Excess pore pressure could have built up at this boundary, driven by the ascent of fluids from the lower SU-2 and SU-1 (Figure 10a and b). The properties of the biogenic carbonate ooze sediments (i.e. low permeability, high water content, fine-grained) defining the substrate of the eventual spread may have a direct contribution to the build-up of pore pressure (Bryn et al., 2005; Kvalstad et al., 2005; Bull et al., 2009b; Urlaub et al., 2015). There is also ample evidence that during the early Miocene to Pliocene, the Exmouth Platform was seismically active, with the Kangaroo Syncline representing an inversion-related structure linked to the collision of the Indo-Australian and Eurasian plates (Keep et al., 2007). Related seismicity may have reduced the shear strength of sediments, and built up the pore fluid pressure within the substrate of MTC 3. The increased pore pressure was transferred laterally westwards away from, and sealed by, the overlying basal shear surface of MTC 1 (Figure 10a) (see also examples of pore pressure lateral propagation from Legget and LaSalle, 1978; Aylsworth and Lawrence, 2003).

Stage 2: Distal evacuation

We suggest that MTC 3 was triggered due to the removal of material from its distal margin by the emplacement of MTC 2. The absence of a buttress after northward transport would have removed the lateral confining pressure within the western part of the pre-spread strata to drive the spreading (Figure 10c). The sediments immediately around the debutressing became a flow (i.e. slump), due to the biogenic structure of carbonate ooze that is rapidly destroyed under loading, transitioning from a coherent to fully disaggregated chaotic mass in a relatively short distance (i.e. 10-20 km; Principaud et al., 2015; Watson et al., 2019).

To the east, the sediment pile was primed to fail for the reasons outlined above (i.e. excess pore pressure; Figure 10a). The low gradient (c. 0.4°) of the basal shear surface of MTC 3 likely prevented the failure from accelerating and translating a great distance during emplacement. As a result, the intra-spread blocks stayed relatively intact compared to failures occurring on

more steeply dipping slopes (i.e. Hengesh et al., 2013). Onshore and offshore data indicate that even small amounts of unloading near the down-dip part of the slope can trigger the formation of spreads (i.e. Kvalstad et al., 2005; Micallef et al., 2007; Locat et al., 2011; Broussard and Sarwar, 2013).

Stage 3: MTC 3 initiation

The mass comprising MTC 3 started sliding westward into the new space created by the movement northwards of MTC 2 (Figure 10c). Additional shearing and deformation below MTC 3 ruptured the base-MTC 1 seal layer, promoting liquefaction of the substrate in over-pressured zone, which drove the upward transport of fluids and the formation of large pipe-like structures.

The tip angle (α) and the friction angle of the block (β) follow a relationship of $\beta \approx 90° - (\alpha/2)$, which aligns with the failure surface angles observed from triaxial experimental tests on intact natural clays (Locat et al., 2011; Locat et al., 2015). This relationship suggests that internal shear fractures were generated during spreading. Two sets of hydraulic internal shear fractures (primary/secondary internal shear fractures) formed and propagated upward due to the high fluid over-pressure in the substrate (Figure 10c). The primary internal shear fractures developed a 'V'-shaped geometry, consistent with the predictions of numerical models of sediment failure (Andresen, 2001; Kvalstad et al., 2005; Dey et al., 2016; Buss et al., 2019). In between the primary internal shear fractures, smaller secondary shear fractures propagated upward from the basal shear surface of MTC 3 (e.g. see also the formation process of the hydraulic fracturing related pipes from Løseth et al., 2011; Cartwright and Santamarina, 2015). The lateral movement of the spread will increase the shear stress in the substrate of MTC 3, driving growth of the primary and secondary fractures. Overlying material was ultimately broken into fracture-bound blocks flanked by troughs.

Stage 4: Internal deformation and lateral spreading

Overpressured substrate fluid-sediment mixes flowed upward via the secondary internal shear fractures within sub-circular fluid pipes (e.g. Cartwright and Santamarina, 2015). This extruded material was deposited in depressions above the troughs on the top surface of MTC 3 (Figure 10d). Blocks near the distal end of MTC 3 underwent a greater lateral displacement and deformation with increase release of the excess pore pressure from the base of the

spread compared to proximal areas that moved less far. Due to the release of overpressure, the shear stress required to drive horizontal motion increased, which may ultimately stop spreading. The spreading may also stop because the mass hit the far (eastern) of the existing MTC 2 lateral margin (Figure 10d). There is an increasing deformation near the headwall of the spread. This is due to the failed sediments of MTC 3 moved west first, this might have ended up with a 'hole' in the east near the initial scarp. The initial scarp was later failed retrogressively, leaving a step-like headwall scarp, and a mass of strongly deformed sediments next to the headwall (Figure 10d).

Implications

Preconditioning and triggering of spreads: Unloading and lubrication

We have investigated the geometry and internal structure of an MTC, inferring it was related to a submarine spread. Our study shows that, in these cases, spreading can occur even if the slope gradient is presently low. We propose that the spread was *primed* by the presence of an overpressured layer, which acts as a basal shear surface and promotes sliding on a very low-angle slope. Slope failure was ultimately *triggered* by debuttressing of the slope mass by an earlier slide, which removed downslope and/or lateral confinement. Together these processes resulted in a short run-out but highly deformed slide mass. While the spread shows abundant evidence for intense internal deformation, we relate this deformation to fluid escape from subsurface overpressured strata beneath the failing mass, rather than to landslide disaggregation under rapid, long-distance transport. We suggest that the slide mass may have only moved a relatively short distance (i.e. only a few hundred metres) and that the amount of strain observed in landslides is therefore not necessarily a direct indication of transport distance.

The importance of rheology and mobility for geohazard assessments

For offshore geohazard assessments it is important to understand the mobility and rheology of an MTC (Thomas et al., 2010). If the landslide mass of MTC 3 moved only a short distance and at relatively low speed, then the potential for tsunamigenesis will be low, despite the relatively large volume (c. 360 km^3) of the mass. Numerical modelling has shown that very large landslides (volumes of up to 1000 km^3) may not trigger a tsunami if they commence as relatively slow, retrogressive failures (Løvholt et al., 2017).

The nature of seafloor and subsurface deformation associated with submarine landsliding control the impact this processes has on different offshore structures. For instance, a seabed-laid pipeline or cable may be able to withstand slow-moving seafloor displacement during a spread, instead being much more vulnerable to the impact of faster-moving slides that become frontally emergent and disaggregate to form more mobile debris flows (Zakeri, 2009; Thomas et al., 2010; Lacroix et al., 2020). Piles or top-hole conductors that support platforms or deep-sea field developments may penetrate tens or hundreds of metres below the seafloor. These deeper foundations are susceptible to i) lateral and vertical movements, which may be relatively limited within intact blocks due to the limited transport distance of the MTC; and ii) changes in subsurface pore pressure and the remoulding of sediments, which together may reduce their lateral capacity (i.e. weakening their support); this particularly property may be prognosed by when an intra-block, fluid vertical fluid venting system is identified (Amaratunga and Grozic, 2009; Hong et al., 2017).

Submarine spreads: Underappreciated agents for seafloor fluid flow

Many studies propose fluid migration at depth as a potential preconditioning or triggering factor for MTCs (e.g. Bünz et al., 2005; Elger et al., 2018; Deville et al., 2020); however, few studies link MTCs to syn- or post-emplacement release of fluids (e.g. Bøe et al., 2012; Browne et al., 2020). It is suggested that significant volumes of methane (an important greenhouse gas) may have been emitted during the disaggregation of the 3000 km^3 Storegga Slide (Paull et al., 2007), and that methane release by widespread submarine landslide activity may have been a contributory mechanism for elevated methane emissions that catalysed the Palaeocene-Eocene Thermal maximum (Higgins and Schrag, 2006). The role of submarine landslides in the release of previously sequestered fluids such as methane remains poorly constrained, and is thus omitted from existing global budgets. Our study shows that fluid escape can play an important role during MTC emplacement, as vertical escape structures act as efficient conduits for fluids and sediments from depth to the seafloor. Similar seafloor fluid expulsions, including that linked to post–MTC emplacement, create cold seeps that support high biomass communities of microbes and chemosynthetic fauna, as the focused fluid flow creates cold seeps (e.g. Deville et al., 2020). Therefore, as well as disturbing the seafloor, MTCs may also provide important hotspots for deep-sea biodiversity, particularly where they create focused zones of fluid flow.

Conclusion

We use 2D and 3D seismic reflection data to investigate processes of submarine spreading, on the Exmouth Plateau, offshore NW Australia. The spread comprises: (i) giant, upward-tapering blocks (c. 300 m-high, c. 1200 m-long, and c. 210 m-wide) which are undeformed, and (ii) intervening troughs (c. 260 m depressions separating the blocks), which are moderately deformed. We interpret that the blocks were only transported minimal lateral distance, and the relatively deformed troughs are formed by the expulsion of fluid and sediment during hydraulic failure of the sediment mass. We then developed a new internal hydraulic fracturing model that accounts for the styles and patterns of blocks and the intervening troughs. The new model requires a low gradient prerequisite over-pressured failure surface/zone, the low gradient of the basal shear surface likely prevented the block from accelerating and translating a great distance during emplacement. The new model suggests that the spread is initiated by the removal of materials in the toe of the otherwise stable strata (i.e. debuttressing). The debuttressing of the adjacent strata results in the decrease of the lateral confining pressure within the pre-spread strata, and subsequently, triggers the spreading process. The underlying overpressured layer is important to prime the spreading and explain the scale and style of fluid escape. An improved understanding of the initiation, emplacement and deposition of submarine spreading failures adds to our broader understanding of deep-water mass failure processes, the risks posed to seafloor infrastructure, and the often-complex interactions with local benthic ecology.

Acknowledgements

The authors would like to thank Geoscience Australia for providing the 2D and 3D seismic reflection data that was used in this study, and Schlumberger are thanked for providing Petrel to Imperial College. The first author thanks the Chinese Scholar Council and iRock Technology for its financial support. The fifth author acknowledges funding from the Natural Environment Research Council CLASS National Capability Programme (NE/R015953/1). The seventh author thanks for funding from Guangdong Basic and Applied Basic Research Foundation (2020B1515020016).

Reference

Alves, T.M., 2015. Submarine slide blocks and associated soft-sediment deformation in deep-water basins: a review. Marine and Petroleum Geology, 67: 262-285.

Amaratunga, A. and Grozic, J., 2009. On the undrained unloading behaviour of gassy sands. Canadian Geotechnical Journal, 46(11): 1267-1276.

Andresen, L., 2001. Effect of strain softening on stability analyses. Analysis of retrogressive sliding due to strain softening—Ormen Lange case study. NGI report(521001-10).

Aylsworth, J. and Lawrence, D., 2003. Earthquake-induced landsliding east of Ottawa; a contribution to the Ottawa Valley Landslide Project, Geohazards 2003, 3rd Canadian Conference on Geotechnique and Natural Hazards/3ième Conférence canadienne sur la géotechnique et les risques naturels; Edmonton, Alberta; CA; June 9-10 juin 2003. Canadian Geotechnical Society.

Bøe, R., Bellec, V.K., Rise, L., Buhl-Mortensen, L., Chand, S. and Thorsnes, T., 2012. Catastrophic fluid escape venting-tunnels and related features associated with large submarine slides on the continental rise off Vesterålen–Troms, North Norway. Marine and petroleum geology, 38(1): 95-103.

Boyd, R., Williamson, P. and Haq, B., 1993. Seismic Stratigraphy and Passive‐Margin Evolution of the Southern Exmouth Plateau. Sequence Stratigraphy and Facies Associations: 579-603.

Bradley, K., Mallick, R., Andikagumi, H., Hubbard, J., Meilianda, E., Switzer, A., Du, N., Brocard, G., Alfian, D. and Benazir, B., 2019. Earthquake-triggered 2018 Palu Valley landslides enabled by wet rice cultivation. Nature Geoscience, 12(11): 935-939.

Broussard, R. and Sarwar, A.K., 2013. A Structural Analysis of the Green Knoll Salt Dome Located in Southeast Green Canyon, Gulf of Mexico.

Brown, A.R., 2011. Interpretation of three-dimensional seismic data. Society of Exploration Geophysicists and American Association of Petroleum Geologists.

Browne, G., Bull, S., Arnot, M., Boyes, A., King, P. and Helle, K., 2020. The role of mass transport deposits contributing to fluid escape: Neogene outcrop and seismic examples from north Taranaki, New Zealand. GML.

Bryn, P., Berg, K., Forsberg, C.F., Solheim, A. and Kvalstad, T.J., 2005. Explaining the Storegga slide. Marine and Petroleum Geology, 22(1): 11-19.

Bull, S., Cartwright, J. and Huuse, M., 2009a. A review of kinematic indicators from mass-transport complexes using 3D seismic data. Marine and Petroleum Geology, 26(7): 1132-1151.

Bull, S., Cartwright, J. and Huuse, M., 2009b. A subsurface evacuation model for submarine slope failure. Basin Research, 21(4): 433-443.

Bünz, S., Mienert, J., Bryn, P. and Berg, K., 2005. Fluid flow impact on slope failure from 3D seismic data: a case study in the Storegga Slide. Basin Research, 17(1): 109-122.

Buss, C., Friedli, B. and Puzrin, A.M., 2019. Kinematic energy balance approach to submarine landslide evolution. Canadian Geotechnical Journal, 56(9): 1351-1365.

Cartwright, J. and Santamarina, C., 2015. Seismic characteristics of fluid escape pipes in sedimentary basins: implications for pipe genesis. Marine and Petroleum Geology, 65: 126-140.

Chaytor, J.D., Baldwin, W.E., Bentley, S.J., Damour, M., Jones, D., Maloney, J., Miner, M.D., Obelcz, J. and Xu, K., 2020. Short-and long-term movement of mudflows of the Mississippi River Delta Front and their known and potential impacts on oil and gas infrastructure. Geological Society, London, Special Publications, 500(1): 587-604.

Chopra, S. and Marfurt, K.J., 2007. Seismic attributes for prospect identification and reservoir characterization. Society of Exploration Geophysicists and European Association of Geoscientists and Engineers.

Clari, P., Cavagna, S., Martire, L. and Hunziker, J., 2004. A Miocene mud volcano and its plumbing system: a chaotic complex revisited (Monferrato, NW Italy). Journal of Sedimentary Research, 74(5): 662-676.

534 Cruden, D.M. and Varnes, D.J., 1996. Landslides: investigation and mitigation. Chapter 3-Landslide
535 types and processes. Transportation research board special report(247).
536 De Blasio, F.V. and Elverhoi, A., 2011. Properties of mass-transport deposits as inferred from
537 dynamic modeling of subaqueous mass wasting: a short review. Mass Transport Deposits in
538 Deepwater Settings: SEPM Special Publication, 96: 499-508.
539 Deville, E., Scalabrin, C., Jouet, G., Cattaneo, A., Battani, A., Noirez, S., Vermesse, H., Olu, K., Corbari,
540 L. and Boulard, M., 2020. Fluid seepage associated with slope destabilization along the
541 Zambezi margin (Mozambique). Marine Geology: 106275.
542 Dey, R., Hawlader, B., Phillips, R. and Soga, K., 2016. Numerical modelling of submarine landslides
543 with sensitive clay layers. Géotechnique, 66(6): 454-468.
544 Dutta, S. and Hawlader, B., 2019. Pipeline–soil–water interaction modelling for submarine landslide
545 impact on suspended offshore pipelines. Géotechnique, 69(1): 29-41.
546 Elger, J., Berndt, C., Rüpke, L., Krastel, S., Gross, F. and Geissler, W.H., 2018. Submarine slope failures
547 due to pipe structure formation. Nature communications, 9(1): 1-6.
548 Exon, N., Haq, B. and Von Rad, U., 1992. Exmouth Plateau revisited: scientific drilling and geological
549 framework, Proceedings of the Ocean Drilling Program, Scientific Results. Ocean Drilling
550 Program College Station, Tex, pp. 3-20.
551 Falvey, D. and Veevers, J., 1974. Physiography of the Exmouth and Scott plateaus, western Australia,
552 and adjacent northeast Wharton Basin. Marine Geology, 17(2): 21-59.
553 Geertsema, M., Blais-Stevens, A., Kwoll, E., Menounos, B., Venditti, J.G., Grenier, A. and Wiebe, K.,
554 2018. Sensitive clay landslide detection and characterization in and around Lakelse Lake,
555 British Columbia, Canada. Sedimentary geology, 364: 217-227.
556 Haq, B.U., Boyd, R.L., Exon, N.F. and von Rad, U., 1992. 47. EVOLUTION OF THE CENTRAL EXMOUTH
557 PLATEAU: A POST-DRILLING PERSPECTIVE1.
558 Hengesh, J., Dirstein, J. and Stanley, A., 2013. Landslide geomorphology along the Exmouth plateau
559 continental margin, North West Shelf, Australia. Australian Geomechanics Journal, 48(4): 71-
560 92.
561 Hengesh, J., Dirstein, J.K. and Stanley, A.J., 2012. Seafloor geomorphology and submarine landslide
562 hazards along the continental slope in the Carnarvon Basin, Exmouth Plateau, North West
563 Shelf, Australia. The APPEA Journal, 52(1): 493-512.
564 Hong, Y., Wang, L., Ng, C.W. and Yang, B., 2017. Effect of initial pore pressure on undrained shear
565 behaviour of fine-grained gassy soil. Canadian Geotechnical Journal, 54(11): 1592-1600.
566 Hull, J. and Griffiths, C., 2002. Sequence stratigraphic evolution of the Albian to Recent section of the
567 Dampier Sub-basin, North West Shelf, Australia, PhD thesis 1999. University of Adelaide,
568 Australia.
569 Jackson, C.A., 2011. Three-dimensional seismic analysis of megaclast deformation within a mass
570 transport deposit; implications for debris flow kinematics. Geology, 39(3): 203-206.
571 Keep, M., Harrowfield, M. and Crowe, W., 2007. The neogene tectonic history of the North West
572 Shelf, Australia. Exploration Geophysics, 38(3): 151-174.
573 Kvalstad, T.J., Andresen, L., Forsberg, C.F., Berg, K., Bryn, P. and Wangen, M., 2005. The Storegga
574 slide: evaluation of triggering sources and slide mechanics. Marine and Petroleum Geology,
575 22(1): 245-256.
576 Lacroix, P., Handwerger, A.L. and Bièvre, G., 2020. Life and death of slow-moving landslides. Nature
577 Reviews Earth & Environment.
578 Lee, S. and Chough, S., 2001. High‐resolution (2–7 kHz) acoustic and geometric characters of
579 submarine creep deposits in the South Korea Plateau, East Sea. Sedimentology, 48(3): 629-
580 644.
581 Legget, R.F. and LaSalle, P., 1978. Soil studies at Shipshaw, Quebec: 1941 and 1969. Canadian
582 Geotechnical Journal, 15(4): 556-564.

583 Li, W., Alves, T.M., Wu, S., Rebesco, M., Zhao, F., Mi, L. and Ma, B., 2016. A giant, submarine creep
584 zone as a precursor of large-scale slope instability offshore the Dongsha Islands (South China
585 Sea). Earth and Planetary Science Letters, 451: 272-284.
586 Locat, A., Leroueil, S., Bernander, S., Demers, D., Jostad, H.P. and Ouehb, L., 2011. Progressive
587 failures in eastern Canadian and Scandinavian sensitive clays. Canadian Geotechnical
588 Journal, 48(11): 1696-1712.
589 Locat, A., Leroueil, S., Fortin, A., Demers, D. and Jostad, H.P., 2015. The 1994 landslide at Sainte-
590 Monique, Quebec: geotechnical investigation and application of progressive failure analysis.
591 Canadian Geotechnical Journal, 52(4): 490-504.
592 Løseth, H., Wensaas, L., Arntsen, B., Hanken, N.-M., Basire, C. and Graue, K., 2011. 1000 m long gas
593 blow-out pipes. Marine and Petroleum Geology, 28(5): 1047-1060.
594 Løvholt, F., Bondevik, S., Laberg, J.S., Kim, J. and Boylan, N., 2017. Some giant submarine landslides
595 do not produce large tsunamis. Geophysical Research Letters, 44(16): 8463-8472.
596 Madhusudhan, B., Clare, M., Clayton, C. and Hunt, J., 2017. Geotechnical profiling of deep-ocean
597 sediments at the AFEN submarine slide complex. Quarterly Journal of Engineering Geology
598 and Hydrogeology, 50(2): 148-157.
599 Maher, B.A. and Thompson, R., 1999. Quaternary climates, environments and magnetism.
600 Cambridge University Press.
601 Masson, D., Harbitz, C., Wynn, R., Pedersen, G. and Løvholt, F., 2006. Submarine landslides:
602 processes, triggers and hazard prediction. Philosophical Transactions of the Royal Society A:
603 Mathematical, Physical and Engineering Sciences, 364(1845): 2009-2039.
604 Micallef, A., Masson, D.G., Berndt, C. and Stow, D.A., 2007. Morphology and mechanics of submarine
605 spreading: A case study from the Storegga Slide. Journal of Geophysical Research: Earth
606 Surface, 112(F3).
607 Moss, J. and Cartwright, J., 2010. 3D seismic expression of km‐scale fluid escape pipes from
608 offshore Namibia. Basin Research, 22(4): 481-501.
609 Nemec, W., 1990. Aspects of sediment movement on steep delta slopes. Coarse-grained deltas, 10:
610 29-73.
611 Nugraha, H.D., Jackson, C.A.-L., Johnson, H.D., Hodgson, D.M. and Clare, M., 2019. How erosive are
612 submarine landslides?
613 Nugraha, H.D., Jackson, C.A.L., Johnson, H.D., Hodgson, D.M. and Reeve, M.T., 2018. Tectonic and
614 oceanographic process interactions archived in Late Cretaceous to Present deep‐marine
615 stratigraphy on the Exmouth Plateau, offshore NW Australia. Basin Research.
616 Ogata, K., Mountjoy, J., Pini, G.A., Festa, A. and Tinterri, R., 2014. Shear zone liquefaction in mass
617 transport deposit emplacement: A multi-scale integration of seismic reflection and outcrop
618 data. Marine Geology, 356: 50-64.
619 Paull, C., Ussler, W. and Holbrook, W., 2007. Assessing methane release from the colossal Storegga
620 submarine landslide. Geophysical research letters, 34(4).
621 Plaza-Faverola, A., Bünz, S. and Mienert, J., 2011. Repeated fluid expulsion through sub-seabed
622 chimneys offshore Norway in response to glacial cycles. Earth and Planetary Science Letters,
623 305(3-4): 297-308.
624 Pope, E.L., Talling, P.J. and Carter, L., 2017. Which earthquakes trigger damaging submarine mass
625 movements: Insights from a global record of submarine cable breaks? Marine Geology, 384:
626 131-146.
627 Posamentier, H.W. and Martinsen, O.J., 2011. The character and genesis of submarine mass-
628 transport deposits: insights from outcrop and 3D seismic data. Mass-transport deposits in
629 deepwater settings: Society for Sedimentary Geology (SEPM) Special Publication 96: 7-38.
630 Principaud, M., Mulder, T., Gillet, H. and Borgomano, J., 2015. Large-scale carbonate submarine
631 mass-wasting along the northwestern slope of the Great Bahama Bank (Bahamas):
632 Morphology, architecture, and mechanisms. Sedimentary Geology, 317: 27-42.

633 Randolph, M.F. and White, D.J., 2012. Interaction forces between pipelines and submarine slides—A
634 geotechnical viewpoint. Ocean Engineering, 48: 32-37.
635 Roberts, K., Davies, R. and Stewart, S., 2010. Structure of exhumed mud volcano feeder complexes,
636 Azerbaijan. Basin Research, 22(4): 439-451.
637 Savage, W.Z. and Varnes, D.J., 1987. Mechanics of gravitational spreading of steep-sided ridges
638 («sackung»). Bulletin of the International Association of Engineering Geology-Bulletin de
639 l'Association Internationale de Géologie de l'Ingénieur, 35(1): 31-36.
640 Scarselli, N., McClay, K. and Elders, C., 2013. Submarine slide and slump complexes, Exmouth
641 Plateau, NW Shelf of Australia, The Sedimentary Basins of Western Australia IV: Proceedings
642 of the Petroleum Exploration Society of Australia Symposium, Perth, WA.
643 Shillington, D.J., Seeber, L., Sorlien, C.C., Steckler, M.S., Kurt, H., Dondurur, D., Cifci, G., Imren, C.,
644 Cormier, M.-H. and McHugh, C., 2012. Evidence for widespread creep on the flanks of the
645 Sea of Marmara transform basin from marine geophysical data. Geology, 40(5): 439-442.
646 Silva, A.J. and Booth, J.S., 1984. Creep behavior of submarine sediments. Geo-marine letters, 4(3-4):
647 215-219.
648 Sobiesiak, M.S., Kneller, B., Alsop, G.I. and Milana, J.P., 2018. Styles of basal interaction beneath
649 mass transport deposits. Marine and Petroleum Geology, 98: 629-639.
650 Strasser, M., Kölling, M., Ferreira, C.d.S., Fink, H.G., Fujiwara, T., Henkel, S., Ikehara, K., Kanamatsu,
651 T., Kawamura, K. and Kodaira, S., 2013. A slump in the trench: Tracking the impact of the
652 2011 Tohoku-Oki earthquake. Geology, 41(8): 935-938.
653 Tappin, D., 2010. Submarine mass failures as tsunami sources: their climate control. Philosophical
654 Transactions of the Royal Society A: Mathematical, Physical and Engineering Sciences,
655 368(1919): 2417-2434.
656 Thomas, S., Hooper, J. and Clare, M., 2010. Constraining geohazards to the past: impact assessment
657 of submarine mass movements on seabed developments, Submarine mass movements and
658 their consequences. Springer, pp. 387-398.
659 Urlaub, M., Talling, P.J. and Masson, D.G., 2013. Timing and frequency of large submarine landslides:
660 implications for understanding triggers and future geohazard. Quaternary Science Reviews,
661 72: 63-82.
662 Urlaub, M., Talling, P.J., Zervos, A. and Masson, D., 2015. What causes large submarine landslides on
663 low gradient (< 2°) continental slopes with slow (~ 0.15 m/kyr) sediment accumulation?
664 Journal of Geophysical Research: Solid Earth, 120(10): 6722-6739.
665 Varnes, D.J., 1978. Slope movement types and processes. Special report, 176: 11-33.
666 Velayatham, T., Holford, S., Bunch, M., King, R. and Magee, C., 2019. 3D Seismic Analysis of Ancient
667 Subsurface Fluid Flow in the Exmouth Plateau, Offshore Western Australia.
668 Velayatham, T., Holford, S.P. and Bunch, M.A., 2018. Ancient fluid flow recorded by remarkably long,
669 buried pockmark trains observed in 3D seismic data, Exmouth Plateau, Northern Carnarvon
670 basin. Marine and Petroleum Geology, 95: 303-313.
671 von Rad, U., Haq, B.U., et al., 1992. Proceedings of the Ocean Program, Scientific Results. Ocean
672 Drilling Program, Leg 122.
673 Watkinson, I.M. and Hall, R., 2019. Impact of communal irrigation on the 2018 Palu earthquake-
674 triggered landslides. Nature Geoscience, 12(11): 940-945.
675 Watson, P., Bransby, F., Delimi, Z.L., Erbrich, C., Randolph, M., Rattley, M., Silva, M., Stevens, B.,
676 Thomas, S. and Westgate, Z., 2019. Foundation design in offshore carbonate sediments–
677 building on knowledge to address future challenges, From Research to Applied Geotechnics:
678 Invited Lectures of the XVI Pan-American Conference on Soil Mechanics and Geotechnical
679 Engineering (XVI PCSMGE), 17-20 November 2019, Cancun, Mexico. IOS Press, pp. 240.
680 Watts, P., Grilli, S.T., Tappin, D.R. and Fryer, G.J., 2005. Tsunami generation by submarine mass
681 failure. II: Predictive equations and case studies. Journal of waterway, port, coastal, and
682 ocean engineering, 131(6): 298-310.

683 Wu, N., Jackson, C.A., Johnson, H. and Hodgson, D.M., 2019. Lithological, petrophysical and seal
684 properties of mass-transport complexes (MTCs), northern Gulf of Mexico. EarthArXiv.
685 February, 19.
686 Zakeri, A., 2009. Review of state-of-the-art: Drag forces on submarine pipelines and piles caused by
687 landslide or debris flow impact. Journal of offshore mechanics and Arctic engineering,
688 131(1).
689 Zhu, H. and Randolph, M.F., 2010. Large deformation finite-element analysis of submarine landslide
690 interaction with embedded pipelines. International Journal of Geomechanics, 10(4): 145-
691 152.

692 Figure caption

693 Figure 1 Schematic diagram showing the classification of mass-transport complexes adopted
694 in this study (modified from Nemec, 1990; Posamentier and Martinsen, 2011; Scarselli et al.,
695 2013).

696 Figure 2 a) Regional map of the study area showing the location of the Exmouth Plateau Arch,
697 Kangaroo Syncline. The white and grey lines represent 2D seismic reflection data, and the red
698 polygon represents the location of 3D seismic reflection dataset. Shaded relief GEBCO_2014
699 bathymetry map downloaded from https://www.ngdc.noaa.gov/maps/autogrid/; b) location
700 map of the figures demonstrated in this study; c) Stratigraphy column and the major tectonic
701 event of the study interval; d) Sketch map of the regional structures crossing the study area,
702 showing the modern depositional systems, adapted from Nugraha et al. (2018).

703 Figure 3 a) Un-interpreted regional seismic section; b) Interpreted regional seismic section
704 highlighting the key horizons and the seismic units the study area, note that the horizon H1 is
705 the same horizon of Horizon C (see detail from Nugraha et al., 2018) which defines an
706 unconformity of late Miocene (~9 Ma); c) Interpretation sketch of the regional seismic section.
707 See Figure 2b for location.

708 Figure 4 a) Regional structure map interpreted based on the 2D and 3D seismic reflection data,
709 showing the depth structure calculated on horizon H3; b) sketch of the regional structure map
710 showing the distribution of the key intervals in SU-3 (undeformed strata, MTC 3, and MTC 2).

711 Figure 5 a) Variance attribute calculated on Horizon H2 within the 3D seismic reflection data
712 area, revealing pipe-like structures. The dashed line indicates the same boundary in Figure 5d
713 between the undeformed and deformed strata. The upper left map shows the zoom-in view
714 of pipe-like structures, and the upper right seismic section shows the seismic cross-section of
715 the fluid pipe; b) depth structure map calculated on basal shear surface of the MTC 3 within

the 3D seismic area; c) variance attribute calculated on Horizon H3 within 3D seismic area; d) sketch of the MTC 3 deposit, revealing the key intervals in SU-3 (undeformed strata, spread, and MTCs).

Figure 6 a) Seismic section showing the eastern boundary of the MTC 3 and the undeformed strata; b) seismic section showing the proximal section of the MTC 3; c) seismic section showing the distal section of the MTC 3. See the location from Figure 5d; d) the calculation of the tip angle (α) of the blocks, and the friction angle of the blocks to the failure surface (β); e) the calculation of height and the spacing of the blocks. See block number from Figure 6b and 6c, and the blocks number refers to the order in which the blocks are away from the undeformed strata.

Figure 7 a) Seismic characteristics of pipe structures in the seismic section with an overlay of the variance attribute, and a zoomed-in view of the VDZs, showing the details of the pipe like fluid escape structures, see the location in Figure 6b; b) variance time slice through the troughs, showing the crater shaped pipes; c) structure map of the horizon H3, showing the top structure of the MTC 3, see the location in Figure 7a. The diameters of the crater-shaped depressions increase upward, from c. 80 m in the variance time slice to hundreds of metres in the structure map.

Figure 8 a) Seismic cross-section through the headwall scarp area of MTC 2; b) seismic cross-section through the lateral margins of MTC 2; c) seismic cross-section through the body of MTC 2.

Figure 9 Stratigraphic evolution of the study area. a) Seismic unit 1 (SU-1), mainly comprises chaotic seismic reflections and deposited as MTCs; b) seismic unit 2 (SU-2), mainly consist of well-layered seismic section and deposited as carbonate drapes; c) the initial stage of seismic unit 3 (SU-3), consist MTC 1 and carbonate drapes; d) the following stage of SU-3, consisting coherent blocks and chaotic intervening troughs; e) the final stage of SU-3, mainly consist erupted sediments which followed by carbonate drapes.

742 Figure 10 Schematic diagram showing the development of the spread: a) Deposition of the
743 undeformed sediments, MTC 1 and down dip evacuation of the MTC 3; b) inferred
744 permeability and shear strength curve through undeformed strata; c) overpressure induced
745 primary and secondary internal fractures propagation stage; d) sediments dislocated into
746 blocks and troughs with extruded sediments deposition stage.

Figure 1

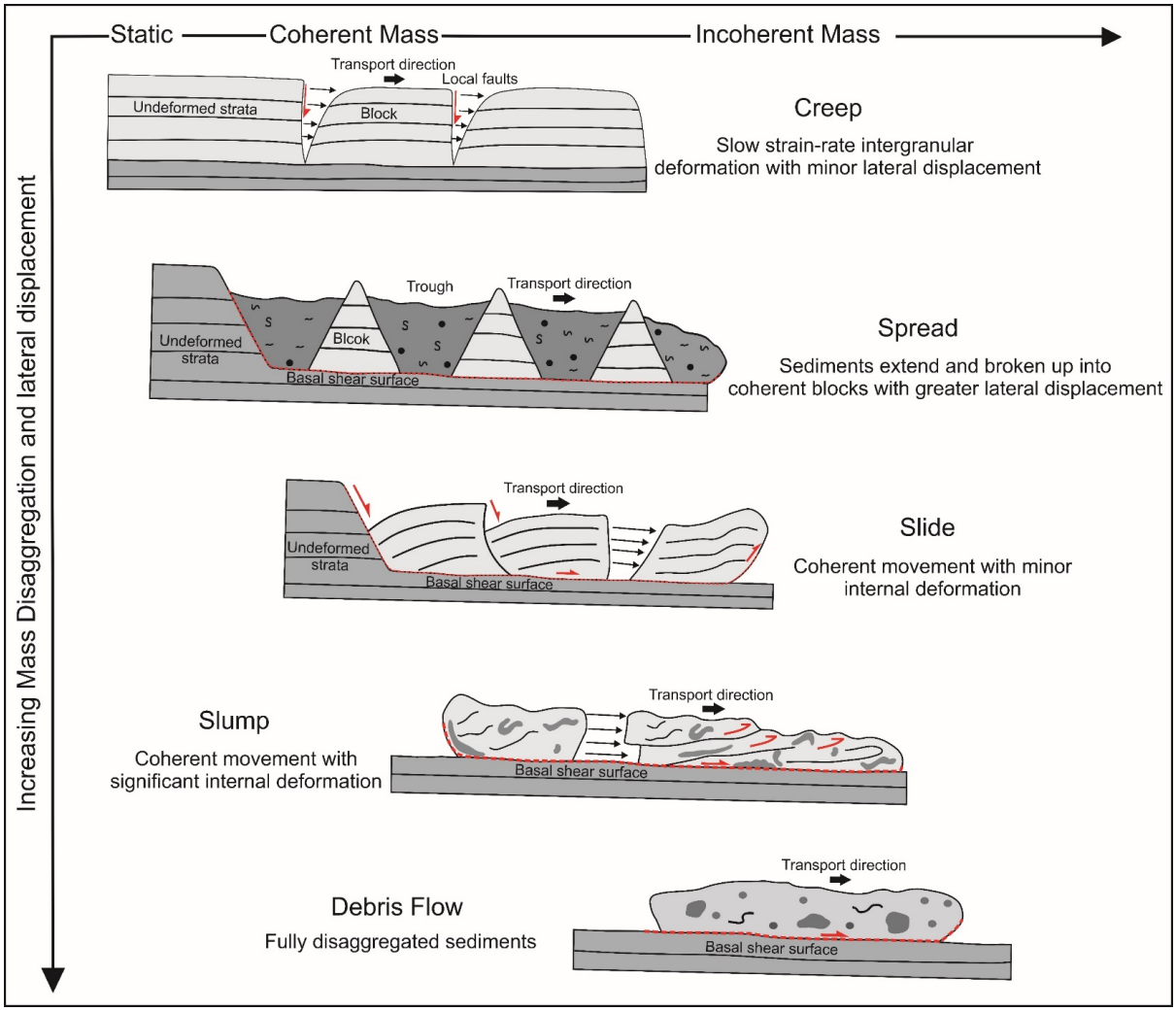
Static
Coherent Mass
Incoherent Mass
Increasing Mass Disaggregation and lateral displacement
Transport direction
Local faults
Undeformed strata
Block
Creep
Slow strain-rate intergranular deformation with minor lateral displacement
Trough
Transport direction
Undeformed strata
Blcok
Basal shear surface
Spread
Sediments extend and broken up into coherent blocks with greater lateral displacement
Transport direction
Undeformed strata
Basal shear surface
Slide
Coherent movement with minor internal deformation
Slump
Coherent movement with significant internal deformation
Transport direction
Basal shear surface
Debris Flow
Fully disaggregated sediments
Transport direction
Basal shear surface

Figure 2

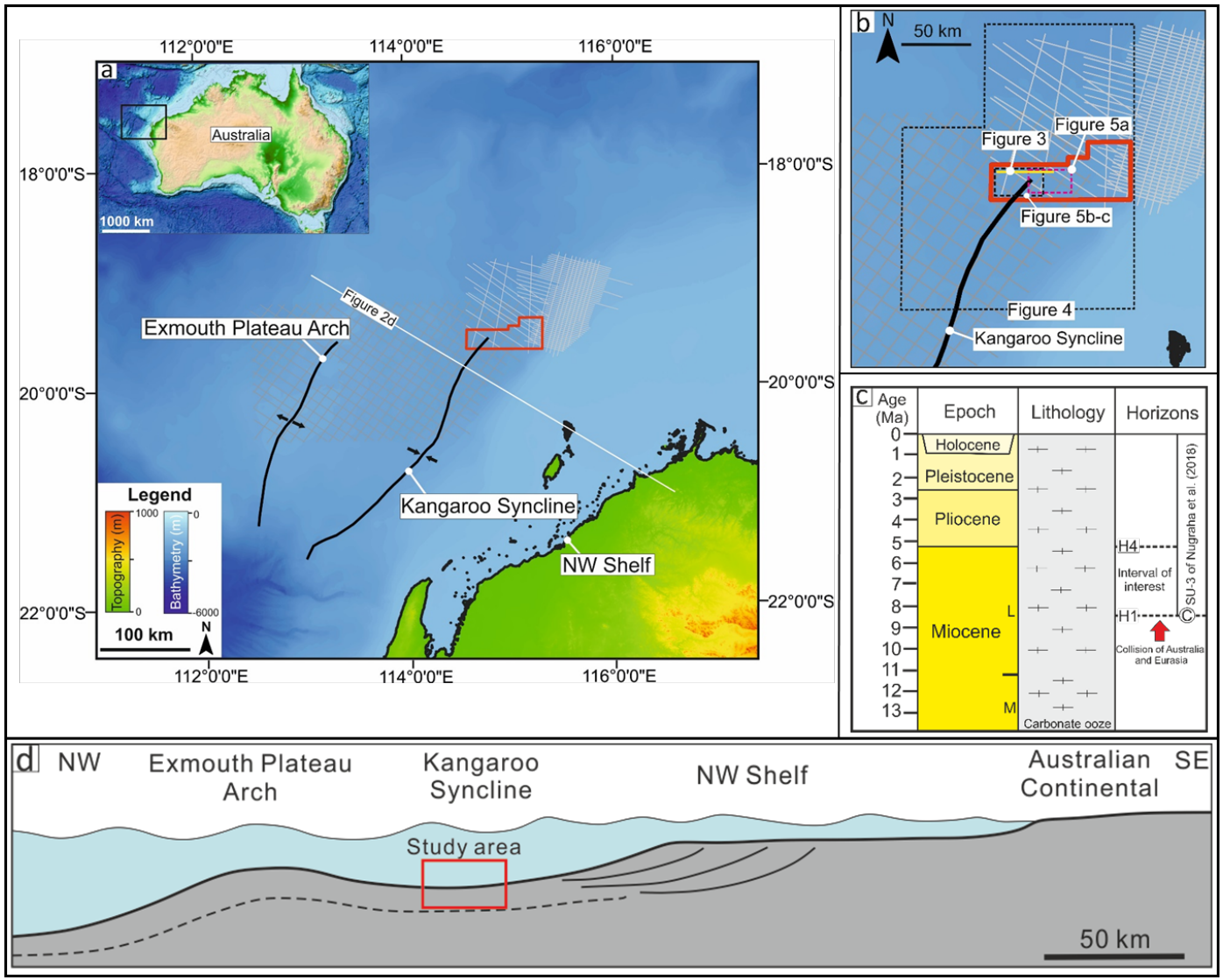
a
112°0'0"E
114°0'0"E
116°0'0"E
18°0'0"S
20°0'0"S
22°0'0"S
Australia
1000 km
Figure 2d
Exmouth Plateau Arch
Kangaroo Syncline
NW Shelf
Legend
Topography (m)
Bathymetry (m)
100 km
N
b
N
50 km
Figure 3
Figure 5a
Figure 5b-c
Figure 4
Kangaroo Syncline
c
Age (Ma)
Epoch
Lithology
Horizons
Holocene
Pleistocene
Pliocene
Miocene
L
M
Carbonate ooze
H4
Interval of interest
H1
SU-3 of Nugraha et al. (2018)
Collision of Australia and Eurasia
d
NW
Exmouth Plateau Arch
Kangaroo Syncline
NW Shelf
Australian Continental
SE
Study area
50 km

Figure 3

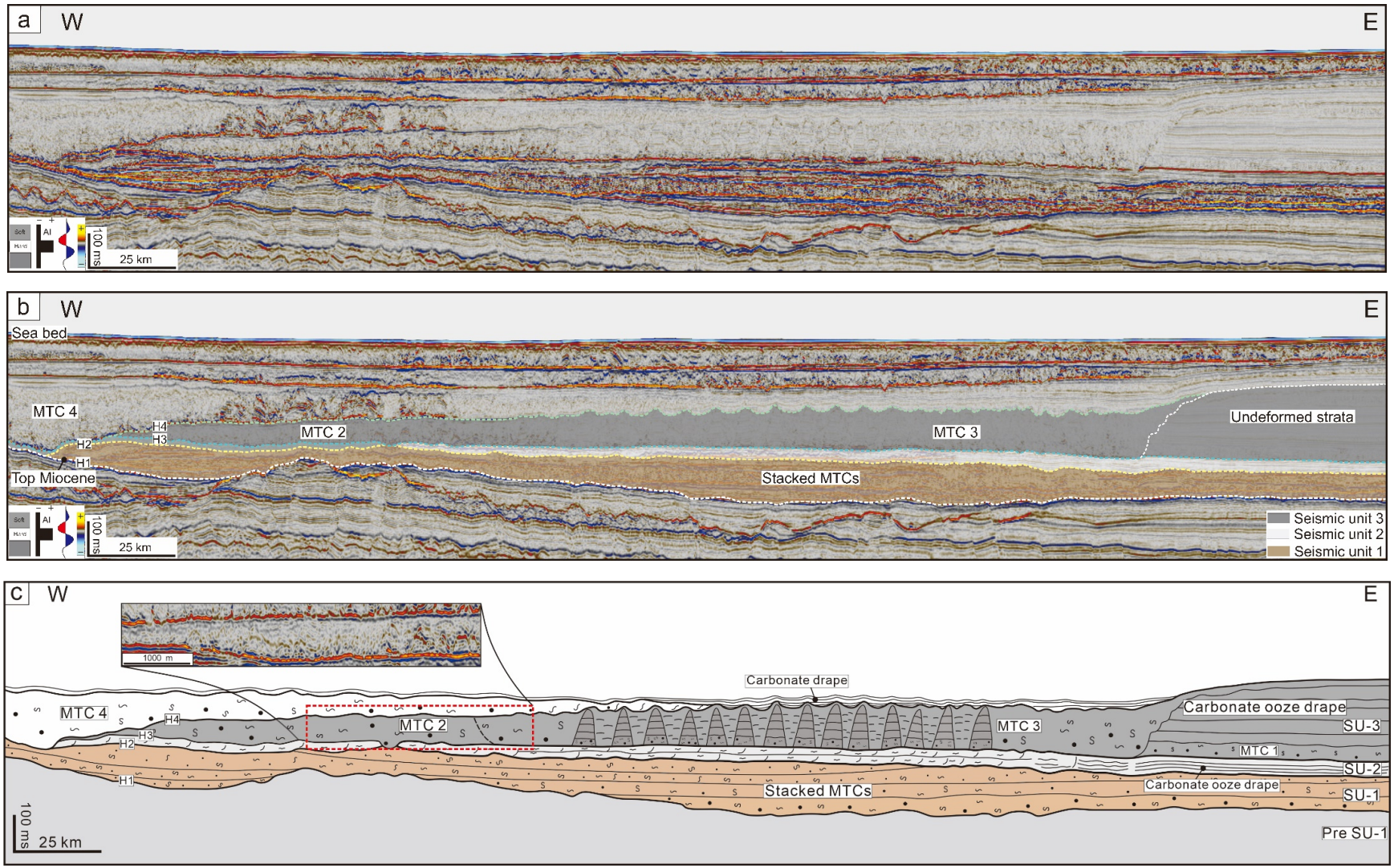
a
W
E
Soft
Hard
AI
100 ms
25 km
b
W
E
Sea bed
MTC 4
H4
H3
H2
H1
MTC 2
MTC 3
Undeformed strata
Top Miocene
Stacked MTCs
Seismic unit 3
Seismic unit 2
Seismic unit 1
c
W
E
1000 m
Carbonate drape
MTC 4
H4
H3
H2
H1
MTC 2
MTC 3
Carbonate ooze drape
SU-3
MTC 1
SU-2
Stacked MTCs
Carbonate ooze drape
SU-1
Pre SU-1
100 ms
25 km

Figure 4

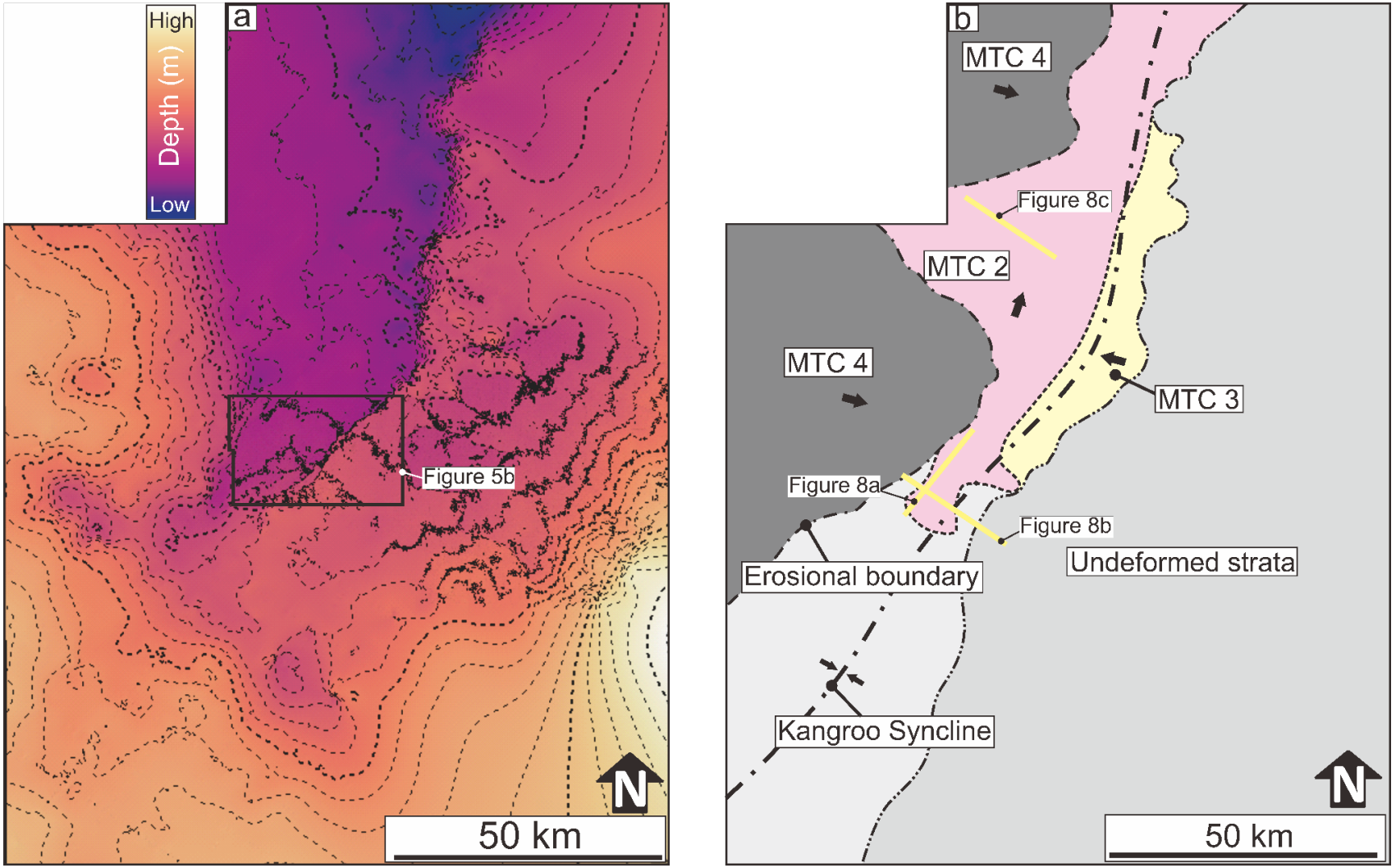
a
High
Depth (m)
Low
Figure 5b
N
50 km
b
MTC 4
Figure 8c
MTC 2
MTC 4
MTC 3
Figure 8a
Figure 8b
Undeformed strata
Erosional boundary
Kangroo Syncline
N
50 km

Figure 5

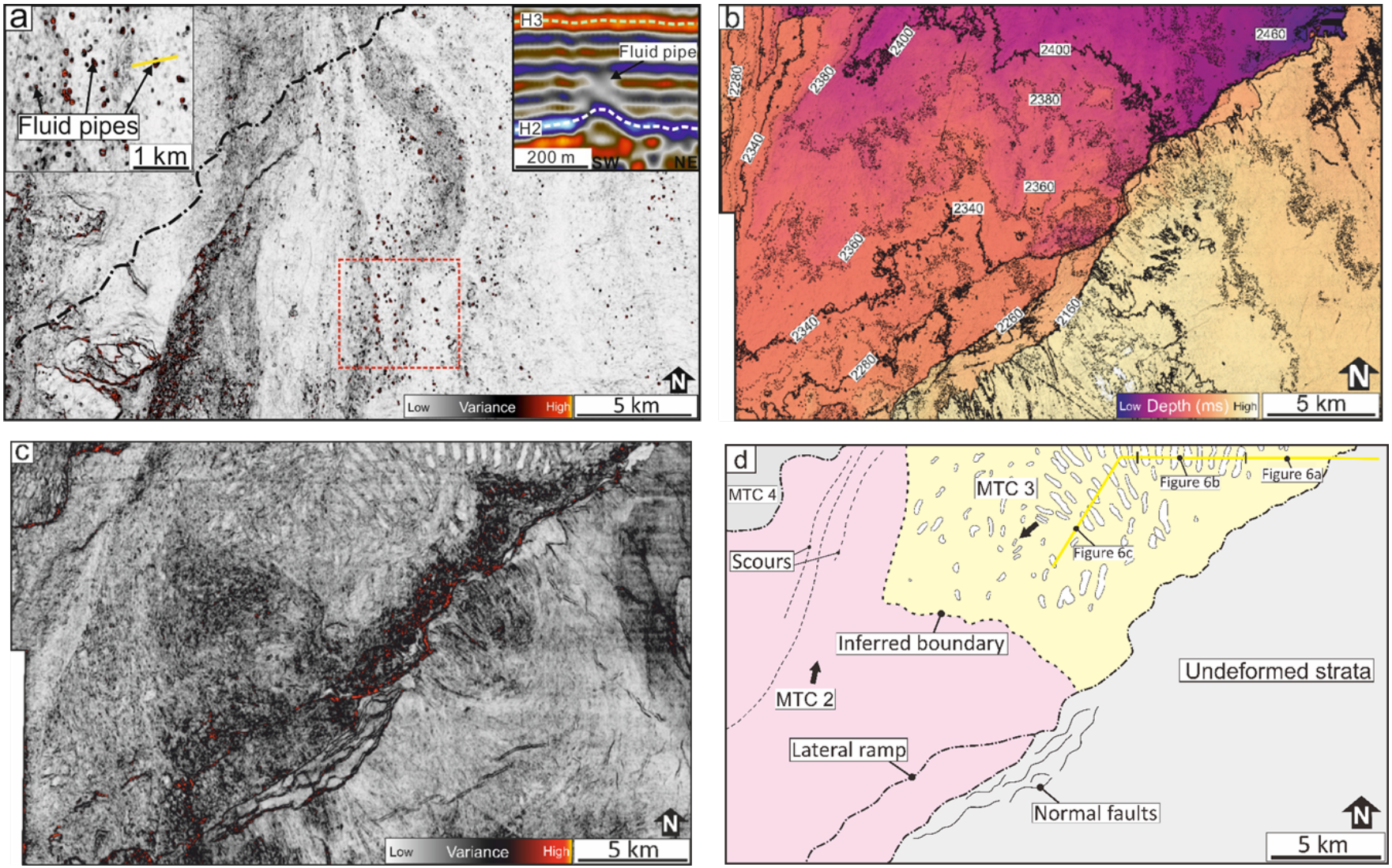
a
Fluid pipes
1 km
H3
Fluid pipe
H2
200 m
SW
NE
Low
Variance
High
5 km
N
b
2460
2400
2380
2340
2360
2280
2260
2180
Low
Depth (ms)
High
5 km
N
c
Low
Variance
High
5 km
N
d
MTC 4
MTC 3
Figure 6b
Figure 6a
Figure 6c
Scours
Inferred boundary
Undeformed strata
MTC 2
Lateral ramp
Normal faults
5 km
N

Figure 6

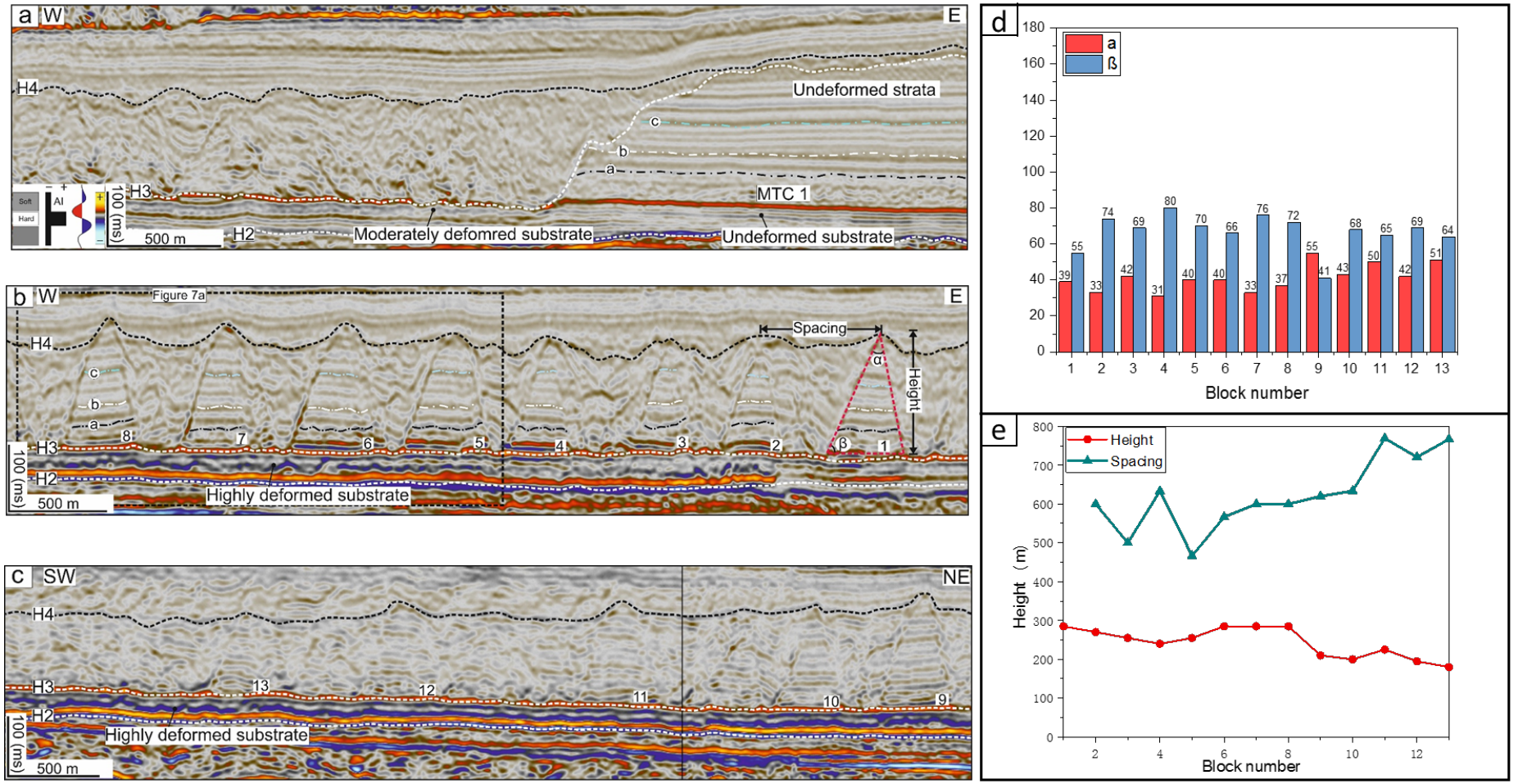
a
W
E
H4
Undeformed strata
c
b
a
H3
MTC 1
Soft
Hard
AI
100 (ms)
500 m
H2
Moderately defomred substrate
Undeformed substrate
b
W
Figure 7a
E
H4
Spacing
α
Height
c
b
a
8
7
6
5
4
3
2
β
1
H3
H2
100 (ms)
500 m
Highly deformed substrate
c
SW
NE
H4
H3
13
12
11
10
9
H2
Highly deformed substrate
100 (ms)
500 m
d
a
ß
180
160
140
120
100
80
60
40
20
0
39
55
33
74
42
69
31
80
40
70
40
66
33
76
37
72
55
41
43
68
50
65
42
69
51
64
1
2
3
4
5
6
7
8
9
10
11
12
13
Block number
e
Height
Spacing
800
700
600
500
400
300
200
100
0
Height (m)
2
4
6
8
10
12
Block number

Figure 7

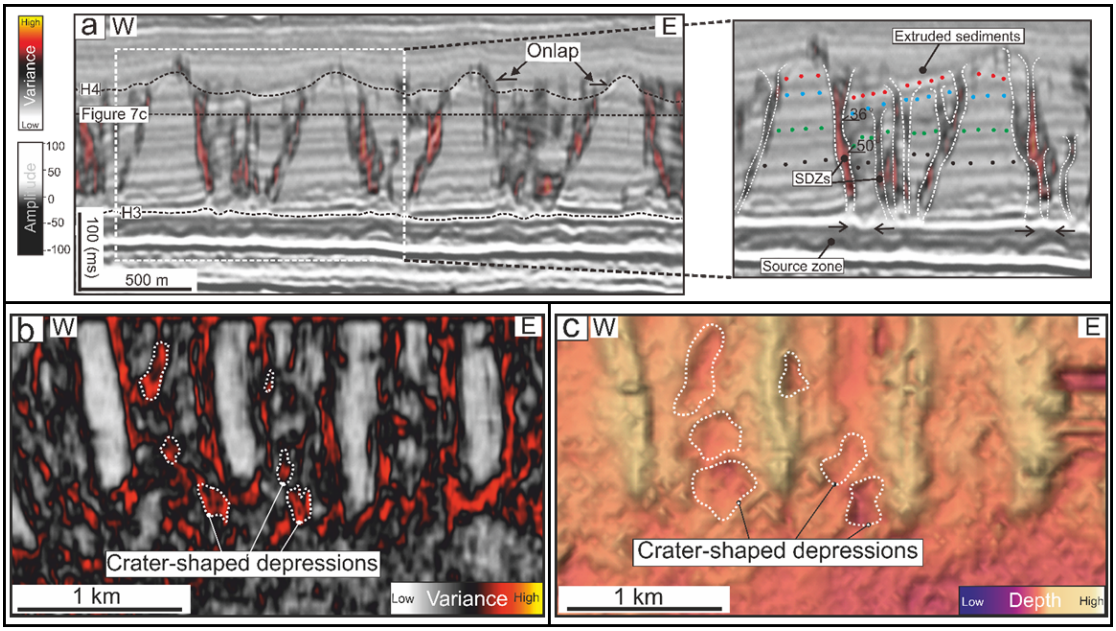
a
W
E
Onlap
H4
Figure 7c
H3
100 (ms)
500 m
High
Variance
Low
100
50
0
-50
-100
Amplitude
Extruded sediments
SDZs
Source zone
b
W
E
Crater-shaped depressions
1 km
Low
Variance
High
c
W
E
Crater-shaped depressions
1 km
Low
Depth
High

Figure 8

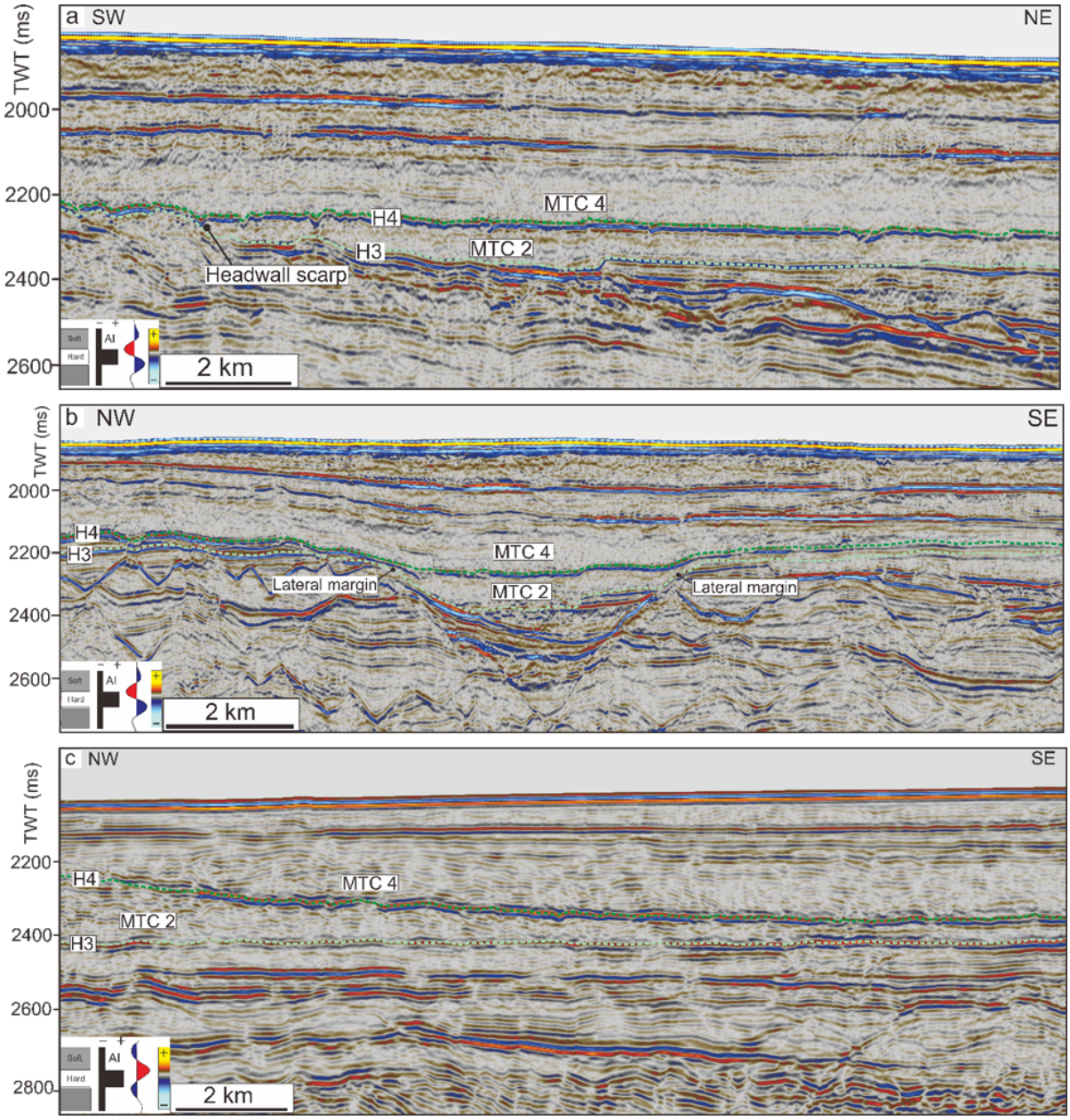
a SW
NE
TWT (ms)
2000
2200
2400
2600
H4
H3
MTC 4
MTC 2
Headwall scarp
2 km
b NW
SE
TWT (ms)
2000
2200
2400
2600
H4
H3
MTC 4
MTC 2
Lateral margin
Lateral margin
2 km
c NW
SE
TWT (ms)
2200
2400
2600
2800
H4
H3
MTC 4
MTC 2
2 km

Figure 9

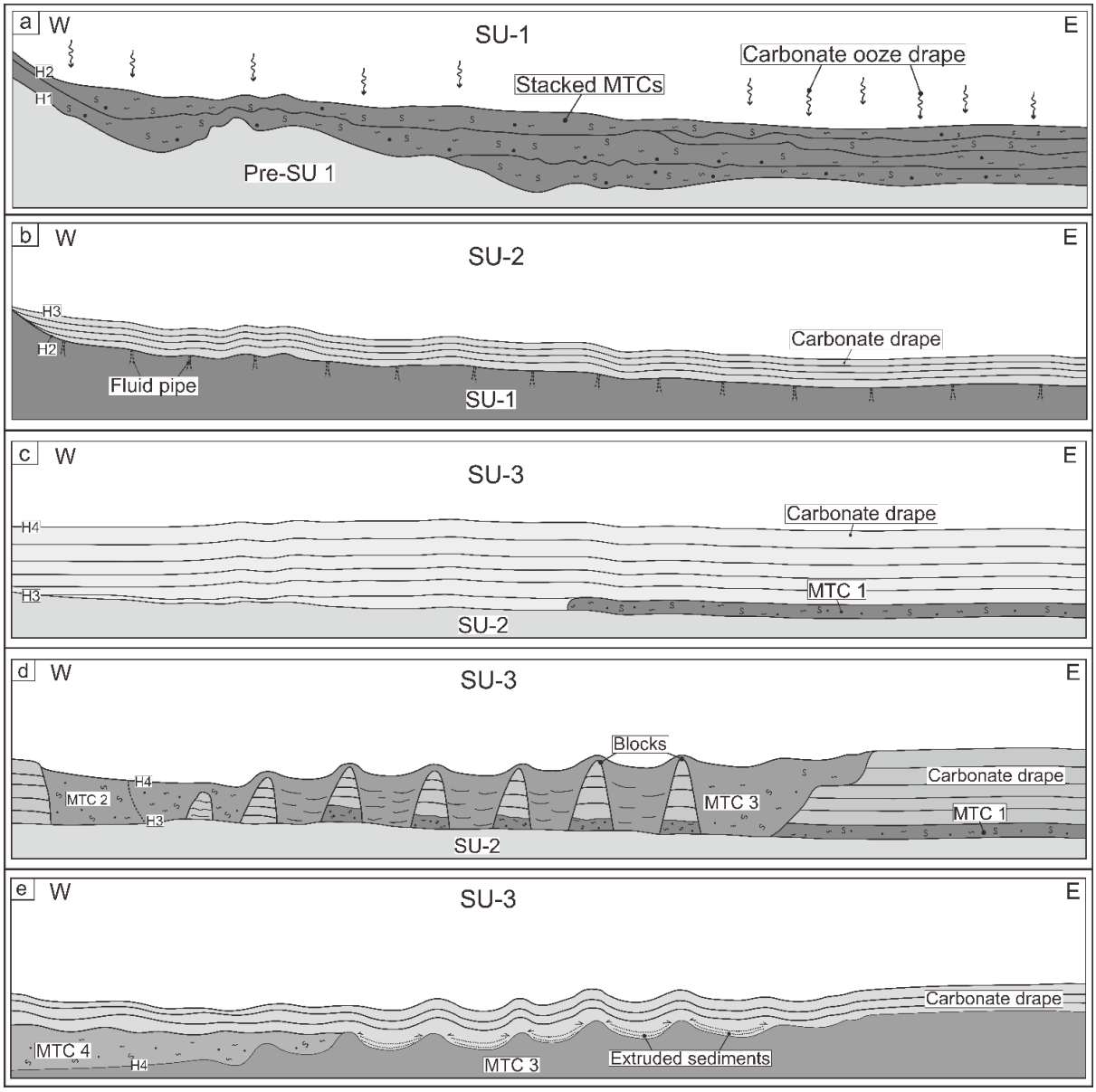
a
W
E
SU-1
Carbonate ooze drape
Stacked MTCs
H2
H1
Pre-SU 1
b
W
E
SU-2
H3
H2
Carbonate drape
Fluid pipe
SU-1
c
W
E
SU-3
Carbonate drape
H4
H3
MTC 1
SU-2
d
W
E
SU-3
Blocks
Carbonate drape
H4
MTC 2
MTC 3
MTC 1
H3
SU-2
e
W
E
SU-3
Carbonate drape
MTC 4
H4
MTC 3
Extruded sediments

Figure 10

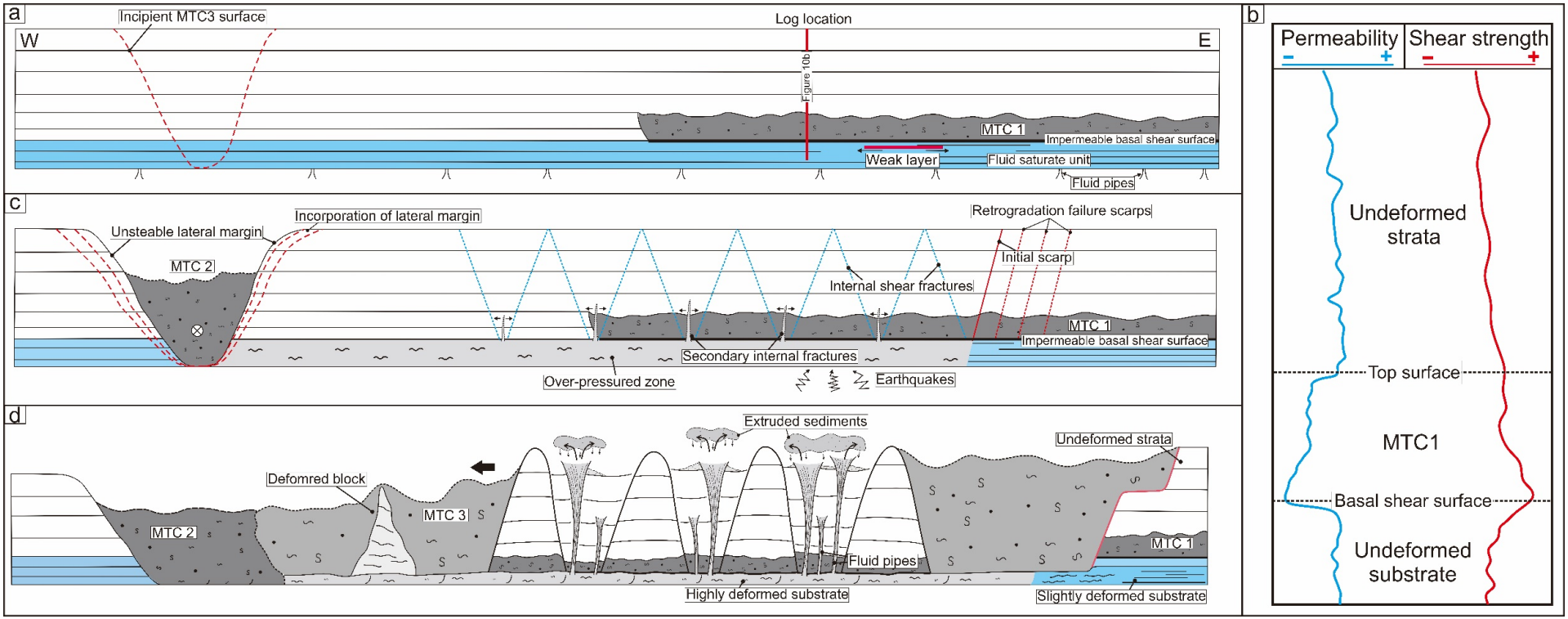
a
Incipient MTC3 surface
W
E
Log location
Figure 10b
MTC 1
Impermeable basal shear surface
Weak layer
Fluid saturate unit
Fluid pipes
c
Unsteable lateral margin
Incorporation of lateral margin
MTC 2
Retrogradation failure scarps
Initial scarp
Internal shear fractures
MTC 1
Impermeable basal shear surface
Secondary internal fractures
Over-pressured zone
Earthquakes
d
Extruded sediments
Undeformed strata
Defomred block
MTC 3
MTC 2
Fluid pipes
MTC 1
Highly deformed substrate
Slightly deformed substrate
b
Permeability
Shear strength
Undeformed strata
Top surface
MTC1
Basal shear surface
Undeformed substrate